Infrared Spectroscopy of Discrete Uranyl Anion Complexes

ARTICLE *in* THE JOURNAL OF PHYSICAL CHEMISTRY A · FEBRUARY 2008

Impact Factor: 2.69 · DOI: 10.1021/jp077309q · Source: PubMed

Infrared Spectroscopy of Discrete Uranyl Anion Complexes

Gary S. Groenewold,* Anita K. Gianotto, and Michael E. McIlwain
Idaho National Laboratory, Idaho Falls, Idaho

Michael J. Van Stipdonk* and Michael Kullman
Wichita State University, Wichita, Kansas

David T. Moore, Nick Polfer, and Jos Oomens
FOM Instituut voor Plasmafysica Rijnhuizen, Nieuwegein, The Netherlands

Ivan Infante and Lucas Visscher
Vrije Universiteit Amsterdam, The Netherlands

Bertrand Siboulet
DEN/DRCP/SCPS, CEA Marcoule, 30207, Bagnols-sur-Cèze cedex, France

Wibe A. de Jong
Pacific Northwest National Laboratory, Richland, Washington

Received: September 11, 2007; In Final Form: October 25, 2007

The Free-Electron Laser for Infrared Experiments (FELIX) was used to study the wavelength-resolved multiple photon photodissociation of discrete, gas-phase uranyl (UO_2^{2+}) complexes containing a single anionic ligand (A), with or without ligated solvent molecules (S). The uranyl antisymmetric and symmetric stretching frequencies were measured for complexes with general formula $[UO_2A(S)_n]^+$, where A was hydroxide, methoxide, or acetate; S was water, ammonia, acetone, or acetonitrile; and $n = 0-3$. The values for the antisymmetric stretching frequency for uranyl ligated with only an anion ($[UO_2A]^+$) were as low or lower than measurements for $[UO_2]^{2+}$ ligated with as many as five strong neutral donor ligands and are comparable to solution-phase values. This result was surprising because initial DFT calculations predicted values that were 30−40 cm^{-1} higher, consistent with intuition but not with the data. Modification of the basis sets and use of alternative functionals improved computational accuracy for the methoxide and acetate complexes, but calculated values for the hydroxide were greater than the measurement regardless of the computational method used. Attachment of a neutral donor ligand S to $[UO_2A]^+$ produced $[UO_2AS]^+$, which produced only very modest changes to the uranyl antisymmetric stretch frequency, and did not universally shift the frequency to lower values. DFT calculations for $[UO_2AS]^+$ were in accord with trends in the data and showed that attachment of the solvent was accommodated by weakening of the U-anion bond as well as the uranyl. When uranyl frequencies were compared for $[UO_2AS]^+$ species having different solvent neutrals, values decreased with increasing neutral nucleophilicity.

Introduction

The chemical behavior of uranium in general, and the linear uranyl dication $[UO_2]^{2+}$ in particular, are diverse on account of the relative ease of redox processes,[1] and the availability of f and d orbitals[2−4] for complex formation. The latter has a profound affect on the solubility of the element.[5,6] In solution, $[UO_2]^{2+}$ is the dominant species,[6−8] where it plays an important role in heavy element separations[9] and in mobility of the element in the environment.[10] At low pH, $[UO_2]^{2+}$ exists as the solvated dication in solution with weakly complexing anions.[10] Hydrolysis[11,12] at higher solution pH values, or the presence of more strongly coordinating anions, produces uranyl complexes coordinated by one or more anionic ligands.[8,13]

The chemical diversity of species has motivated research in vibrational spectroscopy and computational chemistry to understand the coordination and nature of bonding in uranyl complexes containing different ligands because these factors have reactivity and stability implications.[14,15] Infrared and Raman spectroscopy studies of $[UO_2]^{2+}$ have shown that the respective antisymmetric (ν_3) and symmetric (ν_1) stretching frequencies[16] act as convenient "thermometers" for gauging the electron-donating capability of the equatorial ligand field, because the frequencies are strongly correlated with the coordination environment. Nucleophilic ligands in the coordination sphere donate electron density to the cationic metal center, and this spills over into the π^*-antibonding orbitals of the uranyl ion to cause a concomitant decrease in the associated ν_1 and ν_3

* Corresponding authors. E-mail for G.S.G.: gary.groenewold@inl.gov.

10.1021/jp077309q CCC: $40.75
Published on Web 12/29/2007

frequencies. Increased electron density at the uranium metal center can be effected by attachment of more donor ligands,[17] or by increasing the nucleophilicity of the ligands.[18,19] Generally, for a modestly complexing solution environment, ν_3 values near 960 cm^{-1} are typical,[18] as originally reported by Jones and Penneman in 1953.[20] However, when more strongly basic ligands like hydroxide[7,12,21,22] are present, the resulting complexes exhibit much lower ν_3 values, which have been noted in both solutions[23,24] and solids.[25−28] Similar trends for the symmetric ν_1 stretch are seen in Raman spectra[12,15,29] and strong correlations between ν_1 and ν_3 frequencies have been established.[30] Increasing the local electron density at the metal center in other ways, such as by formal reduction (to UO_2^+)[24,31] or substitution of a more electron-rich metal (i.e., Np, Pu, Am), produces a similar effect.[29,32]

Computational chemistry[2,3] helps provide a quantitative understanding of structure and bonding in uranyl complexes. Impressive progress has been made using density functional theory (DFT),[33−36] which is remarkable given the theoretical difficulty of accounting for the large number of electrons, spin−orbit coupling, and relativistic effects encountered in modeling uranyl molecules.[33,35] The computational results are strongly influenced by the choice of functional, basis set, and effective core potential employed.[37,38] Vibrational frequencies generated using DFT[37,39,40] are invaluable because they provide a basis for the interpretation of spectroscopy experiments. However, comparisons between theory and, for example, solution-phase experimental studies are complicated because multiple species may be present in solution[8,41] as a result of rapid ligand exchange, ion pair formation, redox reactions, and solvent effects.[1,7,11,12,17,42] Because vibrational spectra collected from solution-phase experiments potentially contain contributions from multiple species, comparisons to results produced by DFT calculations (which are generated for discrete, well-defined species) are difficult. Longer-range interactions with the second solvation sphere also influence the spectroscopy of the complexes and further complicate comparisons. An elegant way around this is to compare DFT results to structures determined using X-ray crystallography; however, the effect of neighboring molecules in the crystal lattice is a complicating factor.[43]

An alternative approach for converging vibrational spectroscopy and computational chemistry is to measure the infrared spectra of discrete species isolated in the gas phase,[44] which can be accomplished using a trapped ion mass spectrometer (MS) (e.g., a Fourier transform ion cyclotron resonance [FT-ICR] or quadrupole ion trap instrument) interfaced to a high-intensity, tunable infrared source that is provided by a free electron laser.[41,44−47] Using electrospray ionization (ESI),[48−51] a wide range of UO_2^{2+} species[52−55] can be formed and isolated in the FT-ICR-MS. Normally, ion concentrations in the gas phase are too low to enable direct absorption measurements, but by rapid absorption of tens to hundreds of photons, the vibrational energy of a discrete species may be raised to the point where bond cleavage occurs.[44,56] In this case, photon absorption is signaled by a change in ion mass, and plotting ion intensities as a function of wavelength produces infrared multiple photon dissociation (IRMPD) spectra which bear strong similarity to those measured using conventional absorption approaches.[57−59]

In prior research campaigns, the IRMPD strategy was used to produce spectra of discrete uranyl-solvent complexes $[UO_2S_{n=2-5}]^{2+}$ where S = acetone (ACO) and or acetonitrile (ACN).[60] The uranyl ν_3 frequency underwent systematic red shifts with serial addition of donor ligands, and with substitution of a stronger nucleophilic ligand for a weaker one (e.g., ACO for ACN). Interestingly, the uranyl ν_3 frequencies measured using IRMPD were never as low as the value for UO_2^{2+} in solution,[20] despite the fact that the ligands in the gas-phase experiments (ACO and ACN) were stronger nucleophiles than H_2O (the dominant ligand in solution). This observation led to conjecture that additional interactions may be contributing to the observed uranyl shift in solution-phase experiments, an expectation that was recently substantiated using computational methods.[42]

The subject of this report is the IRMPD spectroscopy of gas-phase $[UO_2A]^+$ species (where anion A = OH, OCH_3, and acetate (OAc)), and complexes in which $[UO_2A]^+$ is modified by the attachment of a single neutral donor solvent S, to form $[UO_2AS_{1-2}]^+$ (where S = H_2O, NH_3, ACN, or ACO). The hydroxide and acetate anions are representative of those commonly encountered in solution-phase studies of UO_2^{2+} speciation,[61] and acetate and methoxide are models for functional groups expected to interact with UO_2^{2+} in biological and geochemical environments. The primary focus of this work is to explore and understand the trends in the antisymmetric uranyl stretching frequency (ν_3), as a function of the number and binding strength of the various anionic and neutral ligands, by comparing the experimental IRMPD results with predictions from electronic structure calculations employing several different computational methods. In general, the measured ν_3 frequencies for the bare anion complexes were significantly lower than the predicted computational values and approached those measured in solution for coordinatively saturated UO_2^{2+}. Addition of a neutral donor to form $[UO_2AS]^+$ did not substantially alter the ν_3 values compared to $[UO_2A]^+$, which was surprising because prior studies showed that the antisymmetric stretch is systematically red-shifted upon attachment of a donor neutral ligand. Comparison of the ν_3 values for different $[UO_2AS]^+$ complexes showed a systematic decrease with increasing nucleophilicity of the neutral donor S. DFT calculations also suggested that when the neutral is added, bonding is accommodated by weakening both the uranyl-anion bond, as well as the uranyl moiety.

Experimental Section

IRMPD spectra were collected at the Free Electron Laser for Infrared eXperiments (FELIX) facility, located at the FOM Instituut voor Plasmafysica "Rijnhuizen" (Nieuwegein, The Netherlands).[47] The free electron laser is interfaced to a custom-built Fourier transform ion cyclotron resonance (FT-ICR) mass spectrometer.[57,62]

Generation of Uranyl Complexes by Electrospray Ionization (ESI). ESI was used to generate singly and doubly charged uranyl complexes.[52,54] A one millimolar solution of uranyl nitrate was generated by dissolving the hexahydrate salt (Fluka/Sigma-Aldrich, St. Louis, MO) in water to produce uranyl complexes that were introduced into the hexapole ion accumulation chamber. The ESI source (Micromass, Manchester, U.K.) was operated at 3 kV with respect to ground. Ions were generated at atmospheric pressure and were extracted into vacuum using ion optics oriented orthogonally with respect to the spray axis and then gated into a hexapole ion accumulation chamber where they were stored for 0.5−1.0 s prior to being transmitted into the FT-ICR-MS. The mass spectra observed were sensitive to various temperatures, voltages, and carrier-gas and solution flow rates of the ESI source. Particularly important were the desolvation temperature[54] (which was controlled by a heater and

thermocouple on the block through which the spray capillary passed) and the temperature of the desolvation gas, which were maintained at 29 and 52 °C, respectively. The flow rate of the spray solution was 25 μL min^{-1}, and the desolvation gas (N_2, which ensheathed the solution spray) flow rate was maintained at 30 L min^{-1}. Attempts to make hydrated $[UO_2NO_3]^+$ were not successful because traces of methanol, acetone, acetonitrile, acetic acid, and ammonia in the spray chamber resulted in production of hydroxide, methoxide, and acetate complexes. By increasing the radio frequency power on the ion accumulation hexapole, most of the ion population was converted to $[UO_2OH]^+$, $[UO_2OCH_3]^+$, and $[UO_2OAc]^+$; these species were also formed as complexes with a single solvent molecule (see below), which provided the ensemble of species for infrared spectroscopy.

Fourier Transform Ion Cyclotron Resonance Mass Spectrometry (FT-ICR-MS) and Infrared Multiphoton Dissociation (IRMPD).[46,57,59] Ions accumulated in the external hexapole were gated into the ICR cell, where complexes identified for IRMPD were isolated using a stored waveform inverse Fourier transform (SWIFT) pulse.[63] This ejected all species except those having the desired mass. Isolated ionic complexes were irradiated using two FELIX macropulses, which induced elimination of a solvent molecule, a radical, or a rearrangement product (depending on the complex) when the incident wavelength matched an absorption band. The IRMPD mechanism has been described in detail elsewhere.[45,62,64] Briefly, it involves sequential, non-coherent absorption of many (tens to hundreds) infrared photons, with each photon being "relaxed" by intramolecular vibrational redistribution (IVR) before the next one is absorbed. In this way, the internal vibrational energy of the molecule can be resonantly increased above the dissociation threshold, resulting in fragmentation. It has been shown that the infrared spectra obtained are comparable to those obtained using linear absorption techniques.[56,65] FELIX (60 mJ per macropulse, 5 μs pulse duration, bandwidth 0.2−0.5% of central λ) was scanned primarily through the spectral region of interest around 10 μm, in increments $\leq$0.04 μm, after which IRMPD product ions and un-dissociated precursor ions were measured using the excite/detect sequence of the FT-ICR-MS.[66,67] The IRMPD efficiency was then expressed as $-\log(1 - [\text{summed fragment ion yield}])$, corrected for the width of the acquisition channels and linearly normalized to correct for variations in FELIX power over the spectral range. Peak centers were chosen by fitting a Gaussian peak to the data using Origin plotting software (version 7.5, OriginLab, Northampton, MA). Precision was not evaluated, because of the time required for repetitive acquisition of the peak profiles, and the precious nature of beam time at FELIX. Nevertheless, the precision of measurement of peak position is probably on the order of a couple of cm^{-1}, based on earlier examination of the position(s) of the antisymmetric uranyl stretch and carbonyl C═O stretch in doubly charged complexes.[60]

Because some of the complexes were difficult to fragment, signal-to-noise was less than desired, and so the isolated complexes were subjected to multiple irradiation/acquisition sequences at each wavelength across the scanned region. This lengthened acquisition time, together with the need to strictly economize beam time at the FELIX FT-ICR-MS beamline, constrained data acquisition for most complexes to the diagnostic O═U═O antisymmetric stretch (ν_3).

Density Functional Theory (DFT) Structure and Frequency Calculations. DFT calculations of structures and harmonic frequencies were performed with the DMol^3,[68,69] NWChem,[70,71] Gaussian,[72] and ADF2006.01[73] suite of programs. Different combinations of functionals, basis sets, and relativistic treatments were employed in efforts to derive a consistent view of the IRMPD phenomena measured in the context of complex structure and dissociation behavior. Functionals used were local density approximation (LDA) with the Vosko, Wilk and Nusair (VWN) parametrization,[74,75] the hybrid B3LYP functional,[76,77] and the PW91 functional.[78]

(1) For calculations with DMol^3 the so-called density functional semicore pseudopotential (DSPP)[79] was used, which accounts for scalar relativistic effects and includes 60 electrons in the uranium core (comparable to Stuttgart/Dresden small core ECPs), combined with the use of polarized numerical basis sets (DNP) for the active electrons. A fine (10^{-8}) energy convergence criterion was employed to ensure optimal geometries and representative vibrational frequencies.

(2) For calculations with NWChem and Gaussian, the uranium was described by an effective core potential and its associated basis set: either the LANL2dz ECP and orbital basis set[80] or the MWB60/Stuttgart RSC ECP and basis set (SDD),[81−84] which features Stuttgart/Dresden effective core potentials. Other atoms in the complexes (O, C, H, and N) were described using the aug-cc-pVDZ orbital basis sets,[85] the small D95V basis set,[81−84] the all-electron 3-21g* basis sets, or the 6-31+g(d) basis set. The relatively small basis sets (3-21g (which includes single first polarization functions on row 2 atoms) and D95V) are generally considered to be too small for use in modeling actinide molecules; however, the experimental results and higher-level basis sets used in this study provide a good platform to evaluate the use of the SDD/3-21g* and SDD/D95V general basis set approaches for quick, on-the-spot interpretation of gas-phase IRMPD experiments.

(3) For calculations with ADF, the scalar relativistic ZORA[86] Hamiltonian combined with the TZ2P type basis set was applied within the framework of unrestricted DFT, and a small frozen core that takes 78 electrons in the uranium core and also freezes the 1s electrons of the first row atoms.

NWChem, ADF, and Gaussian were used to compute binding energies and the energetic requirements for different dissociation channels. Prior experience indicated reliable thermodynamic accuracy and thus motivated this approach. For NWChem, the B3LYP energies were obtained using the geometry obtained from LDA geometry optimizations. The energies computed with ADF included spin−orbit coupling terms. The energy differences refer to the fully dissociated limit and hence do not include the additional energy that may be needed to overcome a possible barrier in a transition state (which may be relevant for the loss of H_2O from $[UO_2OH(ACO)]^+$ and photofragmentation of $[UO_2OCH_3]^+$).

In addition, NWChem was used to perform correlation corrected vibrational self-consistent field (cc-VSCF) calculations[87−89] using the LANL2dz basis for uranium, the aug-cc-pVDZ basis sets for the first-row atoms, and the B3LYP functional. These calculations provide an estimate of the effect of anharmonicity and mode-coupling for the fundamental vibrational states. Starting with the VSCF method, degenerate perturbation theory is used to correct for effects of correlation between different vibrational modes, enabling calculation of anharmonic vibrational states for polyatomic molecules.

Finally, we also employed ADF to quantitatively assess the donation of the ligands to the uranyl moiety. The charge transfer between ligands and the uranyl was analyzed using both Hirshfeld charge analysis[90] and Voronoi Deformation Density (VDD) methods.[91]

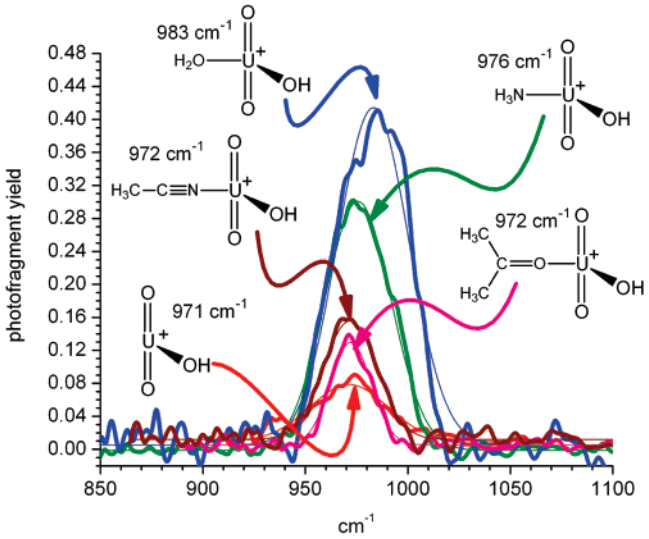

Figure 1. Infrared multiple photon dissociation spectra of the antisymmetric O═U═O stretching region for $[UO_2OH]^+$ and ligand complexes containing (clockwise) a single ACN, H_2O, NH_3, and ACO. The yield values for the ACN complex were multiplied by a factor of 2, to visually distinguish it from the unmodified hydroxide complex.

Results and Discussion

IRMPD of Uranyl−Hydroxide Complexes $[UO_2OH]^+$. Electrospray ionization mass spectrometry of aqueous uranyl nitrate solutions modified with organic solvents had previously been shown to produce dications ligated with neutral donors, provided the capillary temperature was kept close to ambient.[54,60] However, by modestly increasing the capillary temperature and the RF power of the ion accumulation hexapole, uranyl ion pairs were formed that enabled examination of their IRMPD spectra, as a complement to prior measurements made for the uranyl dication bound with neutral ligands.[60] A prominent $[UO_2OH]^+$ ion was produced at *m*/*z* 287, and lower-abundance complexes were observed at *m*/*z* 345, 328, 305, and 304 that correspond to $[UO_2OH(ACO)]^+$, $[UO_2OH(ACN)]^+$, $[UO_2OH(H_2O)]^+$, and $[UO_2OH(NH_3)]^+$, respectively. The ammonia, acetone, and acetonitrile were present in the hexapole accumulation region of the ESI/FT-ICR instrument from prior experiments that involved the use of the solvents and ammonium acetate buffer solutions. The five different hydroxide complexes that were furnished by manipulation of the electrospray conditions were isolated using a SWIFT sequence,[67] and then photofragmented by scanning the free electron laser over the spectral region corresponding to the uranyl antisymmetric stretching frequency (~1000 cm^{-1}); the resulting IRMPD spectra are shown in Figure 1.

Photofragmentation of $[UO_2OH]^+$ resulted in reductive elimination of a hydroxyl radical, and the antisymmetric uranyl ν_3 stretch for this species appeared as a broadened absorption centered at 971 cm^{-1} (Figure 1). The low abundance and profile of the peak reflected inefficient photofragmentation and high energetic requirements:[44] calculations using ZORA/PW91/TZ2P (vide infra) indicated that the minimum energy to dissociate the complex to $[UO_2]^+$ and a hydroxyl radical was 93.9 kcal mol^{-1}. A somewhat smaller dissociation energy of 74.5 kcal/mol was obtained from calculations with the Stuttgart RSC/B3LYP/TZVP combination. The ν_3 value for $[UO_2OH]^+$ was lower than that for the most red-shifted dication complexes $[UO_2(ACO)_4]^{2+}$ (988 cm^{-1}) and $[UO_2(ACN)_5]^{2+}$ (995 cm^{-1}), which suggested at first glance that a single hydroxide transfers as much or more electron density to the uranium center as does four or five strong donors in a fully coordinated uranyl complex. VDD analyses indicated a charge transfer of 0.52 e from the hydroxide to the uranyl, and the charge transfer from four acetones accounted for 0.62 e, suggesting at first glance that the ν_3 values should follow the opposite trend. However, charge transfer would be expected to be more closely correlated with the ν_1 shift, which is influenced purely by electronic factors, and our preliminary estimates indicate that ν_1 would be very similar for both the OH and $(ACO)_4$ complexes.

SCHEME 1: Parallel Elimination Reactions of Isolation and Photofragmentation of $[UO_2OH(ACO)]^+$

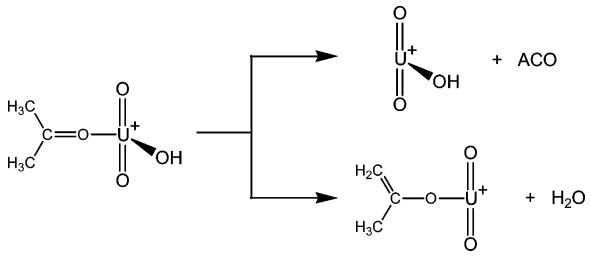

The value for the $[UO_2OH]^+$ uranyl antisymmetric stretching frequency was lower than anticipated on the basis of prior DFT calculations, in which a red shift of 183 cm^{-1} was predicted for $[UO_2(OH)_2]$ by Marsden and co-workers;[40] subtraction of this value from 1140 cm^{-1} (the value calculated for unligated $[UO_2]^{2+}$)[38] produces a frequency of 957 cm^{-1} for the bis-hydroxy complex. The measured value of 971 cm^{-1} for the monohydroxy cannot be compared directly, because the modeled and measured complexes are different. But the values are reasonably close to each other, which suggests that most of the red shift results from attachment of the first OH^- ligand, and that attachment of the second ligand produces a much more modest change in frequency. This trend is in qualitative agreement with very small shifts produced by attachment of neutral donors to $[UO_2A]^+$ complexes (vide infra).

The $[UO_2OH]^+$ ν_3 value measured in the gas phase is very close to that measured in aqueous solution for $[UO_2]^{2+}$ (960−965 cm^{-1}), which is considered to have five inner sphere aquo ligands.[17,18,20,92,93] Lower values have been measured for hydroxide complexes in solution, but these have been attributed to species having multiple uranyl moieties; e.g., a ν_3 measurement at ~940 cm^{-1} has been assigned to $[(UO_2)_2(OH)_2]^{2+}$,[17,21,94] and an even lower ν_3 value of 923 cm^{-1} to $[(UO_2)_3(OH)_5]^+$.[17,94] These ν_3 measurements indicate that the frequency is decreased by the presence of more than one U atom in the complexes but is also certainly influenced by coordinated solvent molecules.

The appearance of $[UO_2OH]^+$ complexed with one or more solvent molecules enabled the effect of neutral donor ligands on the antisymmetric stretching frequency to be examined. The prior study of $[UO_2]^{2+}$ complexes with neutral ligands[60] showed that the antisymmetric stretching frequency was sequentially red-shifted by the serial attachment of additional neutral donor ligands, for example in the acetone (ACO) complexes $[UO_2(ACO)_n]^{2+}$, the frequency decreased from 1017 to 1000 to 988 cm^{-1} as n went from 2 to 3 to 4 (respectively).[60] The trend measured for a series of acetonitrile (ACN) complexes was similar, as was the magnitude of the red shift caused by an additional donor neutral. These observations led to the expectation that attachment of a neutral donor to $[UO_2OH]^+$ would result in a similar red shift.

TABLE 1: Dissociation Energies for IRMPD Reactions of $[UO_2OH(ACO)]^+$ Calculated Using Different Basis Sets

	binding energy (kcal/mol)		
reaction	B3LYP/ LANL2dz/ aug-cc-pVDZ	B3LYP/ Stuttgart RSC/ TZVP	PW91/ ZORA/ TZ2P
$[UO_2OH(ACO)]^+ \rightarrow [UO_2OH]^+ + ACO$	46.5	48.3	41.4
$[UO_2OH(ACO)]^+ \rightarrow [UO_2(OC_3H_5)]^+ + H_2O$	42.6	52.8	41.4

Isolation and photofragmentation of $[UO_2OH(ACO)]^+$ resulted in parallel elimination reactions: loss of intact ACO, and loss of H_2O (Scheme 1, Table 1). Computationally, the two pathways were found to have very similar reaction energies: using ZORA/PW91/TZ2P both channels were endothermic by 41.4 kcal/mol, and a similar conclusion was derived using different basis sets and functionals. The loss of H_2O involves transfer of a proton from a methyl carbon on ACO to the hydroxide, leaving behind the acetone enolate which calculations show remains coordinated through the oxygen atom. No difference in frequencies was observed in the two photofragment channels, which had maxima at 972 cm^{-1}. This value was effectively equal to the measurement for the unmodified $[UO_2OH]^+$, which initially would seem to indicate that addition of the strong ACO donor had no further effect on the uranyl moiety. However, this conclusion is inconsistent with the fairly strong binding of ACO predicted by PW91 and B3LYP calculations, which should shift the uranyl ν_3 value further to the red. Furthermore, the carbonyl stretching region for the $[UO_2OH(ACO)]^+$ complex was scanned and an absorption with a value of 1633 cm^{-1} was found. In our previous study of $[UO_2(ACO)_n]^{2+}$ complexes, we observed that the ligand CO stretch was strongly red-shifted to 1515 cm^{-1} in the $n = 2$ complex, and that this shift decreased with increasing cluster size, to 1583 for $n = 3$ and 1630 for $n = 4$, as the binding energy per ligand was reduced.[60,95] Thus, on the basis of this comparison of carbonyl stretching data, one would expect the binding of the ACO ligand in the $[UO_2OH(ACO)]^+$ complex to be comparable to binding in the $[UO_2(ACO)_4]^{2+}$ complex. Interestingly, addition of a second and third ACO ligand to $[UO_2OH(ACO)]^+$ produced red shifts consistent with the prior experiments. Photofragmentation of $[UO_2OH(ACO)_{n=2,3}]^+$ complexes resulted in the loss of an ACO, with ν_3 values of 961 and 948 cm^{-1} for $n = 2$ and 3, respectively. Therefore, a red shift of 11 cm^{-1} was observed for $n = 1 \rightarrow 2$, and 13 cm^{-1} for $n = 2 \rightarrow 3$; these shifts were in good agreement with the magnitude of the red shifts resulting from ACO addition to the $[UO_2(ACO)_n]^{2+}$ complexes.[60] Taken together, these results suggest that it may be the uranyl antisymmetric stretching frequency in the bare $[UO_2OH]^+$ complex that is anomalously shifted, which is certainly possible given the particular susceptibility of this very small system to anharmonicity effects arising from the IRMPD mechanism. The possible anharmonicity effects are discussed in more detail below.

Isolation of the $[UO_2OH(ACN)]^+$ complex followed by photofragmentation produced elimination of ACN. The antisymmetric UO_2 stretch was measured at 972 cm^{-1}, nearly identical to that for $[UO_2OH(ACO)]^+$ and to $[UO_2OH]^+$. The hydroxide complex with ammonia $[UO_2OH(NH_3)]^+$ underwent photofragmentation solely by loss of NH_3, with a ν_3 value at 976 cm^{-1}, which is slightly *blue*-shifted compared to the unmodified uranyl hydroxide. The final hydroxide complex examined was $[UO_2OH(H_2O)]^+$, which eliminated H_2O upon irradiation that maximized at 983 cm^{-1}, which was 12 cm^{-1} higher than the $[UO_2OH]^+$ value.

The trend for the uranyl ν_3 frequencies for the $[UO_2OH(S)]^+$ complexes were internally self-consistent; i.e., they decreased in the order $H_2O > NH_3 > ACN \sim ACO > (ACO)_2$ (Figure 2). These frequency values are inversely correlated with the calculated coordination energies of different S molecules[40] and are in accord with comparisons of ACO and ACN uranyl complexes.[60] The observed ordering again highlights the remarkably low value measured for unmodified $[UO_2OH]^+$, which would be expected to be higher than 983 cm^{-1} (i.e., the value for the complex with the most weakly bound neutral, $[UO_2OH(H_2O)]^+$). Because it does not seem reasonable to expect that the addition of weakly donating species actually strengthens the uranyl U═O bonds, we must seek other explanations for the blue-shifted bands for the NH_3 and H_2O complexes.

One factor likely contributing to the low ν_3 value for $[UO_2(OH)]^+$ is vibrational anharmonicity derived from the multiple photon absorption process. Red shifts in the spectra of the *para*-aminobenzoic acid[58] and $[CeOH(ACO)_3]^{2+}$ cations[95] have been attributed to IRMPD anharmonicity, and the same phenomenon may contribute to the low frequency measured for $[UO_2OH]^+$. These studies demonstrate that when molecules or complexes attain very high internal energies via the IRMPD process, their vibrational bands exhibit non-negligible red shifts. This can be particularly dramatic for systems with low densities of states,[44] such as the $[UO_2OH]^+$ complex studied here, which only has nine vibrational modes. The energy required to dissociate $[UO_2OH]^+$ to $[UO_2]^+$ and a hydroxyl radical was evaluated computationally, and both the Stuttgart RSC ECP and the ADF TZ2P basis sets produced high values (Table 2). This was consistent with the fact that hydroxide had the highest coordination energy of any ligand in the extensive compilation calculated by Marsden and co-workers.[40] These considerations support the

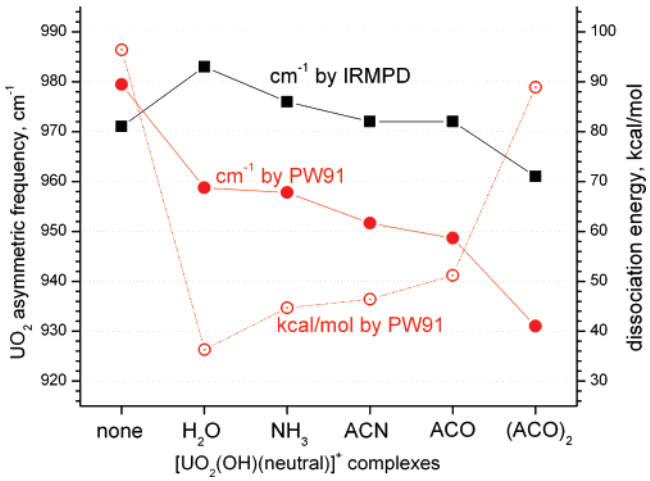

Figure 2. Variation in the antisymmetric O═U═O stretching frequencies for $[UO_2(OH)]^+$ and $[UO_2(OH)(neutral)]^+$ complexes. Black squares are IRMPD measurements, and filled red dots are ν_3 values calculated using PW91, both evaluated using the left *y* axis. Open red circles represent dissociation energies for the complexes, calculated using PW91 and evaluated with the right *y* axis.

TABLE 2: Dissociation Energies Calculated for IRMPD of $[UO_2OH]^+ \rightarrow [UO_2]^+ + OH$

reaction	binding energy (kcal/mol^{-1}) B3LYP/ Stuttgart RSC/ TZVP	PW91/ ZORA/ TZ2P
dissociation from the singlet ground state	74.5	93.9
dissociation from a triplet excited state	30.7	

attribution of the anomalously low $[UO_2OH]^+$ ν_3 value to anharmonicity effects. Another possible explanation is that the dissociation proceeds via a low-lying electronically excited state. The lowest triplet excited state, which should be accessible via spin−orbit coupling, lies ~31 kcal mol^{-1} (calculated using B3LYP and the Stuttgart RSC/TZVP basis) below the dissociation limit.

In contrast to the small $[UO_2OH]^+$ molecule, more complex systems containing a neutral ligand tend to have reduced dissociation energies and a significantly higher vibrational density of states. For example, water binds to the $[UO_2OH]^+$ complex by only 30 kcal/mol, while doubling the number of vibrational modes, three of which are low-frequency intermolecular modes that may contribute disproportionately to the vibrational density of states. This may explain why the ν_3 frequencies of the $[UO_2OH(S)]^+$ complexes are not apparently affected by anharmonicity, compared to the bare $[UO_2OH]^+$ which is strongly shifted by anharmonicity induced by the IRMPD process. A ν_3 value unshifted by anharmonicity would be expected to be ~990 cm^{-1} for $[UO_2OH]^+$ to be consistent with the trend in the ν_3 bands of the $[UO_2OH(S)]^+$ complexes measured here.

Correlation corrected vibrational SCF (cc-VSCF) calculations can provide a rough estimate of whether or not differential red-shifting would be expected in comparing $[UO_2OH]^+$ and $[UO_2OH(S)]^+$ complexes. The cc-VSCF estimates the effect of anharmonicity by including coupling between the lower vibrational modes calculated in the harmonic approximation. Factoring in an influence by anharmonicity, the calculated ν_3 value for $[UO_2OH]^+$ decreased by 10 cm^{-1} (from 987 cm^{-1} in the harmonic approximation to 977 cm^{-1} with the anharmonic corrections), which would account for part of the expected red shift for the hydroxide seen in the IRMPD data. However, the shift calculated for $[UO_2OH(H_2O)]^+$ was very nearly the same at 8 cm^{-1} (going from 968 to 960 cm^{-1} with anharmonic corrections), so the differential anharmonic shift calculated for $[UO_2OH]^+$ and $[UO_2OH(H_2O)]^+$ does not explain the low ν_3 value measured for $[UO_2OH]^+$. It should be noted that the cc-VSCF calculations only consider coupling of the lowest ~10 vibrational levels, whereas coupling and population of the higher excitation levels would certainly be expected to contribute at the high excitation energies achieved in the IRMPD experiments.

As mentioned above, participation of an electronically excited state for $[UO_2OH]^+$ could also contribute to the apparently low ν_3 frequency. The energy calculated for promotion of an electron into the lowest excited triplet state calculated using both LANL2dz/B3LYP/aug-cc-pVDZ and scalar ZORA/PW91/TZ2P using unrestricted DFT was ~45 kcal/mol, which is less than that calculated to dissociate $[UO_2OH]^+$ (except when the LANL2dz basis set was used). If vibrational-to-electronic transitions are indeed occurring in the multiple photon photodissociation experiments, then a lowered frequency would be expected for the electronically excited molecule.[96] The ν_3 value calculated for $[UO_2OH]^+$ in this lowest excited state was quite

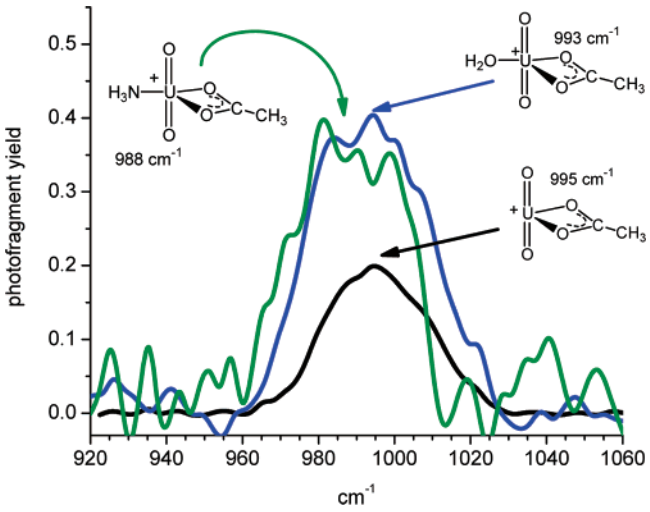

Figure 3. Infrared multiple photon dissociation spectra of the antisymmetric O=U=O stretching region for $[UO_2OAc]^+$ and ligand complexes containing a single NH_3 and H_2O.

a bit lower, at 908 cm^{-1}, and the broadening of the hydroxide profile might thus be the result of overlap of absorptions of ground-state and excited-state molecules. It should also be noted that this triplet state can be considered a complex of reduced uranyl $[UO_2]^+$and neutral hydroxyl radical and is hence directly related to the observed dissociation pathway.

IRMPD of Uranyl−Acetate Complexes $[UO_2OAc]^+$. ESI produced a relatively abundant ion at *m*/*z* 329, which was attributed to uranyl acetate $[UO_2OAc]^+$, that was formed from residual acetic acid that had been used to enhance the protonated ion formation from peptide and protein solutions in previous experiments at FELIX. Because acetate is a stronger conjugate base, it replaces nitrate in the ion accumulation chamber prior to injection into the FT-ICR-MS. The composition was confirmed by accurate mass measurement and the photofragmentation pathway observed in the IRMPD experiment, in which a neutral loss of 42 mass units (presumably as ketene) furnished $[UO_2OH]^+$ as the product ion. For IRMPD of $[UO_2OAc]^+$ the maximum for the antisymmetric uranyl stretch was 995 cm^{-1} (Figure 3), higher than any of the hydroxide complexes measured. This is consistent with the fact that acetate is a weaker gas-phase base[97] than either hydroxide or methoxide (vide infra) and consequently is also likely to be a weaker uranophile. Despite the presumed lower basicity, the antisymmetric uranyl stretching frequency for $[UO_2OAc]^+$ appeared at a value lower than that for nearly all of the uranyl dication complexes ligated with multiple neutral donor ligands reported earlier.[60] In solution, acetate complexes have been the subject of several infrared studies, and the most appropriate value for the antisymmetric stretch to use in a comparison is 954 cm^{-1}, which was measured by Quiles[17] for $[UO_2OAc]^+$. This value is significantly lower than the IRMPD measurement, which reflects the attachment of additional solvent ligands to the $[UO_2OAc]^+$ metal center. Other studies have produced values that ranged as low as 919 cm^{-1},[18,23] but these measurements probably contain contributions from species that contain more than one acetate ligand, and the possibility of variable acetate coordination.[17] Recently, DFT using the LDA functional was used by de Jong and co-workers to calculate uranyl ν_3 value for $[UO_2OAc]^+$ at 1025 cm^{-1}.[98] A careful examination of the carbonyl stretching frequencies could provide insight into this and will be investigated in further experimental campaigns.

Also observed in the ESI spectrum were low-abundance ions at *m*/*z* 346 and 347 that corresponded to ammonia and water

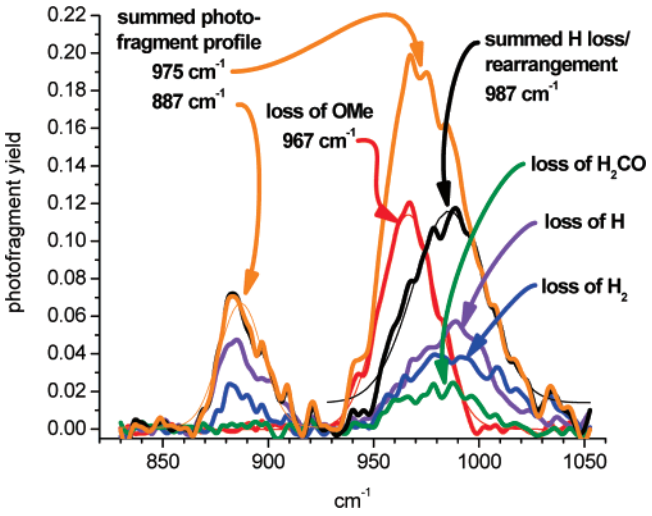

Figure 4. Infrared multiple photon dissociation spectra of the symmetric and antisymmetric O═U═O ν_3 stretching region for $[UO_2OCH_3]^+$. The orange trace represents the spectrum generated by the summed photofragment abundance, red represents the OCH_3 radical elimination, violet represents the H radical elimination, blue represents the H_2 elimination, green represents the H_2CO elimination, and black represents the sum of the H-loss/rearrangement related channels.

complexes (respectively), having compositions $[UO_2OAc(NH_3)]^+$ and $[UO_2OAc(H_2O)]^+$. Photofragmentation of these complexes involved elimination of either NH_3 or H_2O, producing $[UO_2OAc]^+$ in each case. Consistent with prior studies of donors, the antisymmetric UO_2 stretching frequency was red-shifted for both H_2O and NH_3 complexes relative to $[UO_2OAc]^+$, although the magnitude of the shifts were small: the value for the H_2O complex at 993 cm^{-1} was lower by 2 cm^{-1}, and a shift of 7 to 988 cm^{-1} was observed for the NH_3 complex. The trend in the measured frequencies indicate that both H_2O and NH_3 are donating electron density, and that NH_3 is a stronger uranophile than is H_2O, consistent with Marsden's prior DFT results,[40] the relative order of proton affinities,[97] and bonding to other metal cations.[99] The fact that the frequency of the unmodified acetate is very close to that of both ligand complexes suggests that the frequency for the $[UO_2OAc]^+$ complex may also be red shifted as a result of anharmonicity. However, the effect is less pronounced than in the case of the hydroxide complex, as indicated by the fact that the ν_3 of the unmodified $[UO_2OAc]^+$ complex is not lower than the values of the H_2O and NH_3 adducts. Compared to the hydroxide complex, a smaller anharmonic red shift for OAc is consistent with a higher density of states,[44] and with a lower-energy requirement for fragmentation of the acetate complex, which involves rearrangement rather than direct bond-cleavage and elimination of a radical.

IRMPD of Uranyl−Methoxide Complexes $[UO_2OCH_3]^+$. The accurate mass measurement of the ion at *m*/*z* 301 confirmed the composition of uranyl methoxide, which was formed by reaction of uranyl ion with methanol that was present in the ESI solution. Photofragmentation of $[UO_2OCH_3]^+$ produced four different product ions corresponding to the elimination of the OCH_3 and H radicals, H_2, and H_2CO (Scheme 2).

The IRMPD spectrum of the methoxide complex contained two bands, with maxima at 975 and 887 cm^{-1} (Figure 4, orange trace). DFT calculations (B3LYP/Stuttgart RSC/3-21G*) indicated that the higher frequency corresponded to overlapped antisymmetric uranyl ν_3 and C−O stretching bands, and the lower frequency to the symmetric uranyl ν_1 band normally observed in the Raman spectrum.[7,12,15,22,29] The appearance of

SCHEME 2: Photofragmentation of $[UO_2OCH_3]^+$ Yielding Four Different Product Ions Corresponding to the Elimination of the OCH_3 and H Radicals, H_2, and H_2CO

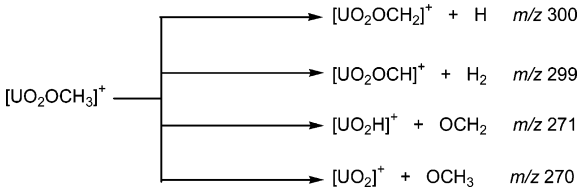

the symmetric stretch indicates a lowered symmetry in the complex, resulting from strong binding of the methoxide that perturbs the linearity of the uranyl functional group. This was supported by the lowest-energy structures and bond angles produced by B3LYP calculations (vide infra).

Striking differences were observed when comparing the IR spectra produced using the different photodissociation channels. The spectrum generated by monitoring the loss of the OCH_3 radical contained a single sharply defined peak with a maximum at 967 cm^{-1}, a frequency slightly lower than that measured for the uranyl antisymmetric stretch for the unmodified hydroxide complex, and consistent with the fact that methoxide is a stronger base than is hydroxide. The peak centered at 967 cm^{-1} was not observed in the spectra generated by the other three fragmentation channels, either because it is not occurring in these channels or because it was overlapped with the O−C stretch (see below). If the latter is true, then it suggests that the ν_3 frequency in the spectrum of the OCH_3 loss channel is red-shifted by about 20 cm^{-1} due to the higher energetic requirements for that channel; shifts of this magnitude have been observed previously.[58]

The IR spectra generated from the photodissociation channels corresponding to the loss of either H or H_2 bore strong similarities to one another in that they contained a peak with a maximum at 987 cm^{-1} and a second peak at about 887 cm^{-1}. The higher-frequency peak probably contains components from the unresolved uranyl asymmetric stretch and C−O stretching, and the lower-frequency peak corresponds to the symmetric UO_2 stretch. The IR spectrum generated by the H_2CO elimination was similar to the H-loss spectra but lacked the band for the symmetric stretch. The appearance of very dissimilar IR spectra in the different photodissociation channels was remarkable, because IRMPD spectra generated from competing mass channels are normally identical or are very similar, with the fragmentation channels having the higher energetic requirements being modestly red-shifted as a result of anharmonicity that results from population of higher vibrational levels when multiple photons are serially absorbed.[58,95] Fast intramolecular vibrational redistribution randomizes the deposited energy regardless of the frequency of initial deposition, and thus the competing fragmentation channels display similar if not identical IR spectra.[56]

A hypothetical interpretation of these observations is that the order of reaction endothermicities for the four reactions is $-H_2 \sim -H < -OCH_2 < -OCH_3$. In the IR spectra generated by losses of H and H_2, peaks are seen in all three absorption modes, symmetric uranyl, asymmetric uranyl, and C−O (assuming that the asymmetric uranyl and C−O are overlapping). The symmetric uranyl and C−O are weakly absorbing modes and hence are only seen in those eliminations having low-energy requirements. The spectrum generated by loss of OCH_2 contains the asymmetric uranyl and perhaps the C−O, but the energetic requirement for this channel is too high to enable observation

TABLE 3: Calculated Enthalpies for the Dissociation Reactions of $[UO_2OCH_3]^+$ (Scheme 2)

	binding energy (kcal/mol^{-1})		
reaction	B3LYP/ Stuttgart RSC/ 6-31+G(d)	B3LYP/ Stuttgart RSC/ (TZVP)	PW91/ ZORA/ (TZ2P)[a]
$[UO_2OCH_3]^+ \rightarrow H_2 + [UO_2(OCH)]^+$	52.8	52.7	52.3
$[UO_2OCH_3]^+ \rightarrow H + [UO_2(OCH_2)]^+$	67.3	73.7	74.8
$[UO_2OCH_3]^+ \rightarrow OCH_3 + [UO_2]^+$	68.4	69.8	83.3
$[UO_2OCH_3]^+ \rightarrow OCH_2 + [UO_2(H)]^+$ (H linear, triplet spin state)	59.0	58.1	
$[UO_2OCH_3]^+ \rightarrow OCH_2 + [UO_2(H)]^+$ (H linear, singlet spin state)		85.2	
$[UO_2\text{-}OCH_3]^+ \rightarrow OCH_2 + [UO_2(H)]^+$ (H equatorial)	79.9	80.7	85.6

[a] ZORA numbers include spin−orbit interaction.

of the symmetric uranyl stretch. The higher energetic requirements are probably related to the fact that the product ion has to be reduced, forming either a U(IV) species $[UOOH]^+$ or a uranyl hydride $[UO_2(H)]^+$. Finally, the spectrum generated by loss of OCH_3 contains only the antisymmetric uranyl peak, because the energetics for this reaction are higher, which means that it can only be accessed via the high-intensity ν_3 uranyl absorption. This peak is substantially red-shifted as a consequence of the large number of photons that must be deposited for the reaction to occur. Further, the presumed rapid rate for OCH_3 radical loss reduces observation of the slower, lower-energy losses.

Enthalpy changes calculated for the different fragmentation channels displayed some agreement with this hypothesis. B3LYP and PW91 calculations using different core approximations, functionals, and basis sets (Table 3) showed that elimination of H_2 was the lowest. The losses of the radical species H and OCH_3 were next and appeared to be roughly energetically competitive, depending on computational approach; the PW91 calculations suggest that loss of OCH_3 requires more energy than loss of H radical, and B3LYP gives somewhat smaller dissociation energies and has the H elimination channel slightly above the OCH_3 elimination channel. Enthalpy requirements for the loss of H_2CO vary depending on the nature of the product ion. Both B3LYP calculations indicate that formation of a linear, triplet $[UO(OH)]^+$ is lowest, within about 7 kcal mol^{-1} of H_2 loss, but when a singlet is formed, or when the product is uranyl coordinated with an equatorial hydride, fragmentation enthalpies were higher. In summary, the PW91 energetics supports the idea that loss of OCH_3 radical is higher in energy and thus more susceptible to anharmonic shifting. However, the variations in the reaction energies seen when comparing the computational approaches do not allow us to state the energetic order of the elimination reactions unequivocally.

An alternative explanation would be the existence of two or more isomers of $[UO_2OCH_3]^+$; however, DFT calculations did not support the existence of energetically competitive isomers, although rearrangement may be occurring during the IRMPD process. An alternative structure that was considered contained an H atom bound to uranium, with formaldehyde equatorially coordinated: for such a structure an absorption corresponding to carbonyl group should be observed, but a survey of the 1500−1700 cm^{-1} wavelength region did not show an additional peak. Thus, a structure involving a bound formaldehyde ligand is unlikely, as our prior studies[60,95] showed that the C═O stretch can be readily detected in complexes with carbonyl-containing ligands.

Involvement of an excited state for the uranyl methoxide can also be argued, which would be expected to have energetic requirements similar to the 45 kcal/mol required for the hydroxide complex. Intuitively, this is an attractive explanation because a higher-spin species would be expected to have a higher propensity for rearrangement and elimination of H and OCH_3 radicals. When the energetic requirement for conversion to a triplet excited state was calculated using PW91, it was also found to be 45 kcal mol^{-1}, in a range that would be accessible during the IRMPD photofragmentation. However, as in the two previously offered rationalizations, this too remains speculative at the present time, and hence an unequivocal identification of the origin of the differences in the spectra of the different mass channels is still elusive.

The assignment of the higher frequency to a C−O stretch drew support from the spectra acquired for the $[UO_2OCH_3\text{-}(H_2O)]^+$ and $[UO_2OCH_3(NH_3)]^+$ adducts (Figure 5). The three peaks in the spectra of these complexes had frequencies consistent with the spectra of unmodified $[UO_2OCH_3]^+$. In the adduct ions, photofragmentation of the methoxide ligand did not occur; instead, only the energetically favored losses of H_2O or NH_3 were observed.

The frequencies measured for the antisymmetric UO_2 stretch for the H_2O and NH_3 complexes were modestly red-shifted compared to the maximum value for the summed photofragment channels of the unmodified $[UO_2OCH_3]^+$, and the trend

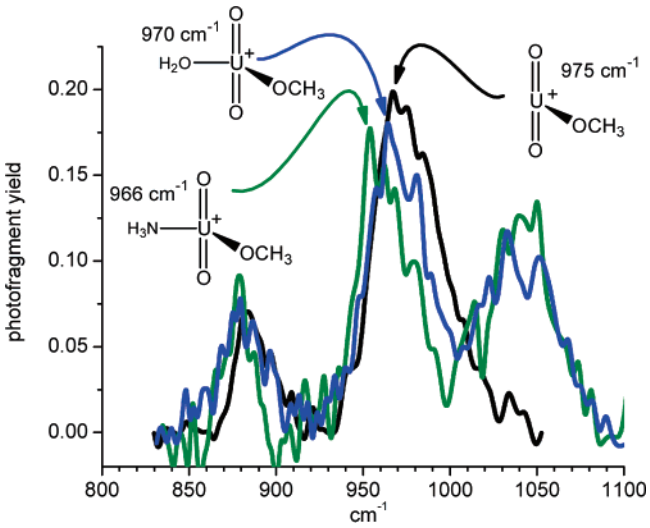

Figure 5. Infrared multiple photon dissociation spectra of the antisymmetric O═U═O stretching region for $[UO_2OCH_3]^+$ (black trace, sum of all photofragment channels), $[UO_2OCH_3(H_2O)]^+$ (blue trace, scaled by 0.55), and $[UO_2OCH_3(NH_3)]^+$ (green trace scaled by 0.6). The photofragment yield for the H_2O and NH_3 complexes was higher than for the unmodified methoxide complex, and scaling was performed to facilitate comparison.

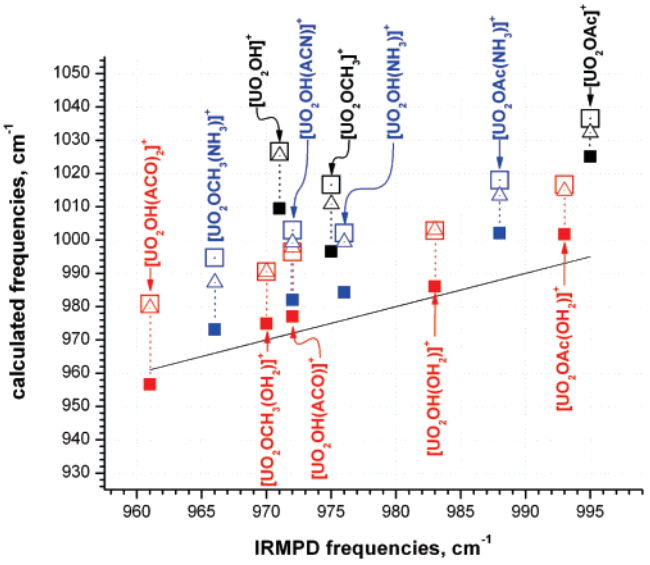

Figure 6. Uranyl ν_3 frequencies calculated using B3LYP plotted versus IRMPD measurements. The line represents the experimental data. Filled square data points were generated using the SDD pseudopotential approach (Stuttgart RSC ECP on U, D95V on C, H, N, and O) elements. Values represented by open squares were generated using Stuttgart RSC ECP for uranium and 3-21g* for C, H, N, and O, and values represented by open triangles utilized 6-31+g(d) for C, H, N, and O. Black points represent $[UO_2(anion)]^+$ complexes with no neutral donor, red represents those with O-donating neutrals, and blue represents those with N-donating neutrals.

observed is consistent with what would be expected for addition of a second weak donor ligand (H_2O), and then substitution of a slightly more basic ligand NH_3 for H_2O. Similarly, the frequencies measured for the symmetric stretch were very similar for all three complexes: the ν_1 value for the unmodified $[UO_2OCH_3]^+$ was measured at 887 cm^{-1}, and the peak position is only very modestly shifted to 880 cm^{-1} when H_2O is attached, and to 879 cm^{-1} for NH_3. These values are about 20 cm^{-1} higher than ν_1 values measured for solvated $[UO_2OAc]^+$ using Raman spectroscopy.[12] As in the case of the hydroxide complexes, the uranyl stretching frequencies of the methoxide complexes were not significantly red-shifted by addition of a neutral donor ligand. This suggests that in the unmodified methoxide complex $[UO_2OCH_3]^+$, the uranyl frequency may be shifted to a lower value as a result of anharmonicity, in a fashion similar to that suspected to be occurring in the hydroxide complexes. As noted, red-shifting would be facilitated by high energetic requirements for the elimination reaction in the unmodified $[UO_2OCH_3]^+$ or by participation of an excited state.

Although addition of a second donor ligand does not cause large changes in the uranyl stretching frequencies,[43,98] it appears to strengthen the C−O bond in the methoxide ligand. This would be expected if the methoxide were modestly repelled by attachment of H_2O or NH_3 to the uranium center. In the spectra for both $[UO_2OCH_3(H_2O)]^+$ and $[UO_2OCH_3(NH_3)]^+$, the C−O stretch was observed at ca. 1038 and 1040 cm^{-1}, shifted to higher frequency by ~50 cm^{-1} compared to unmodified $[UO_2OCH_3]^+$. This trend is directly analogous to what was observed in the IR spectra of discrete uranyl acetone dication complexes: when an additional donor ligand was added, the binding of all equatorial ligands was weakened, and the C═O stretching frequency increased, approaching that of free acetone;[60] in the present case, it is the C−O stretch of methoxide that is increased. Calculations also suggested loosening of the U−OCH_3 bond upon ligation with a neutral donor.

Comparisons of Calculated Frequencies. The changes in vibrational frequencies can be understood in part by comparison with frequencies, bond lengths, and angles calculated using density functional theory. Because calculations of complexes containing actinide elements are challenging, different combinations of functionals and basis sets were used. These results provided multiple opportunities for comparison with measurements, in particular using the antisymmetric uranyl stretch, which was the salient figure of merit in this study. A comparison of the uranyl frequencies calculated using B3LYP with different basis sets versus the IRMPD measurements (Figure 6, Table 4) showed that overall the smallest errors were obtained using the SDD/D95V approach (Stuttgart RSC for U, D95V for all other elements). This agreement might be somewhat fortuitous due to cancellation of errors, considering the D95V basis sets do not have polarization functions. The LDA/DSPP/DNP results are also in reasonable agreement, though some of the calculated trends are incorrect. Calculated values using Stuttgart RSC on U and 3-21g* and 6-31+g(d) for C, H, N, and O were systematically 20−30 cm^{-1} higher than measurements for the solvent complexes, depending on the donor. Overall, differences between the two sets of calculations were small, but the values calculated using 6-31+g(d) were slightly better than those generated using 3-21g* where some trends were incorrect. The data in Figure 6 may be grouped into three categories: anion complexes with no donor, with an O-donor (H_2O or acetone), or with an N-donor (NH_3 or acetonitrile). Calculations for the O-donor anion complexes were in best agreement with experiments, being within a few cm^{-1} when the SDD/D95V approach was used, and on the order of 20 cm^{-1} high when the Stuttgart RSC/3-21g* and Stuttgart RSC/6-31+g(d) approaches were

TABLE 4: Uranyl Antisymmetric Stretching Frequencies (ν_3) for Complexes $[UO_2AS_{0,1,2}]^+$, Generated Using IRMPD, and Calculated Using the Same B3LYP, LDA, and PW91 Functionals, Comparing Various Basis Sets

A (anion)	S (neutral solvent)	IRMPD measurements	B3LYP/ Stuttgart RSC/ D95V	B3LYP/ Stuttgart RSC/ 3-21g*	B3LYP/ Stuttgart RSC/ 6-31+g(d)	B3LYP/ Stuttgart RSC/RLC/ TZVP	LDA/ DSPP/ DNP	LDA/ Stuttgart RSC/ TZVP	PW91/ Stuttgart RSC/ TZVP	PW91/ ZORA/ TZ2P
OH		971	1009	1027	1025	1035	995	1017	987	979
OH	H_2O	983	986	1003	1003	1015	973	1001	969	959
OH	NH_3	976	984	1002	999	1011	973	990	962	958
OH	CAN	972	982	1003	999		973			952
OH	ACO	972	977	996	998		968			949
OH	2 ACO	961	957	981	980		939			931
OAc		995	1025	1037	1032		995			987
OAc	H_2O	993	1002	1017	1015		984			970
OAc	NH_3	988	1002	1018	1013		986			966
OCH_3		975	997	1017	1011	1018	979	1003	973	964
OCH_3	H_2O	970	975	990	990	994	961	997	954	943
OCH_3	NH_3	966	973	995	987	994	959	980	950	944

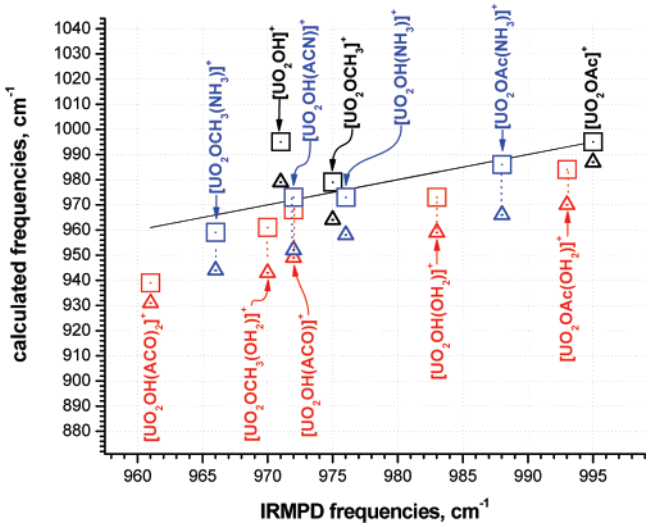

Figure 7. Uranyl ν_3 frequencies calculated using LDA/DSPP/DNP and PW91/ZORA/TZ2P, plotted versus IRMPD measurements. The line represents the experimental data. The open squares were generated using LDA/DSPP/DNP, and the triangles were generated using PW91/ZORA/TZ2P. The black points represent $[UO_2A]^+$ complexes with no neutral donor, red corresponds to complexes with O-coordinating neutrals, and blue corresponds to those with N-coordinating neutrals.

used. Calculations for the complexes containing a neutral that coordinates via an N atom were slightly less accurate, with differences ranging from 5−10 cm^{-1} for the Stuttgart RSC/D95V approach to ∼30 cm^{-1} using the other basis sets for the first row elements. This suggests that N-donation is slightly more aggressive in the gas-phase experiment than predicted by theory. Calculations for the $[UO_2(anion)]^+$ complexes containing no neutral donor displayed the poorest agreement with experiment, being 20 to nearly 60 cm^{-1} higher than the measurements, depending on the basis set used. The poorer agreement likely reflects the high energetic requirements for photofragmentation pathways for these complexes, which is reasonable because they involve elimination of an oxy radical with concomitant reduction of the uranium center. The need to vibrationally excite the uranyl-anion complexes to a higher level increases the opportunity for the measured ν_3 value to be shifted lower as a result of vibrational anharmonicity, or perhaps by participation of an excited state, as suggested above.

In contrast, calculations using LDA and PW91 functionals produced uranyl ν_3 frequencies that were slightly lower than measurements (Figure 7). The LDA/DSPP/DNP values (Figure 7, open squares) were generally in good agreement with measurement, with the salient exception of $[UO_2OH]^+$. Compared to experiments, the LDA values for anion complexes with O-donating ligands were systematically lower than values for complexes with N-donors, by about 10 cm^{-1}. The value calculated for the $[UO_2OH(ACO)_2]^+$ was ca. 20 cm^{-1} lower than the measured value.

The frequencies generated with PW91/ZORA/TZ2P were in general lower than those generated using LDA/DSPP/DNP or B3LYP, consistent with our earlier work on the neutral donor ligands.[60] The ligand induced shifts are very similar to the results obtained with the other approaches, however, and systematic differences between O- and N-donors were not calculated.

Additional insight into the potential interactions from anion binding can be gained by examining the changes in the calculated bond lengths and angles, which would also check the internal consistency of the predicted stretching frequencies. We selected the calculations performed using B3LYP/Stuttgart RSC/6-31+g(d) for discussing relationships between calculated bond lengths and frequencies, which are listed in Table 5, and trends in bond lengths with varying ligation are depicted graphically in Figure 8 (detailed structural parameters generated using B3LYP with three different basis sets are contained in Supplementary Tables S1− S12, and visual representations are provided in Figures 8−10). As ligands are added, calculations show that all distances within the uranyl coordination sphere increase. The magnitude of the increase depends not only on the nucleophilic strength of the different ligands but also on their volumes, and the calculations provide a means to develop a more quantitative assessment of the effect of ligand addition to uranyl. The O═U═O bond length is represented by the lower three traces in Figure 10, and the effect of the anion A, and

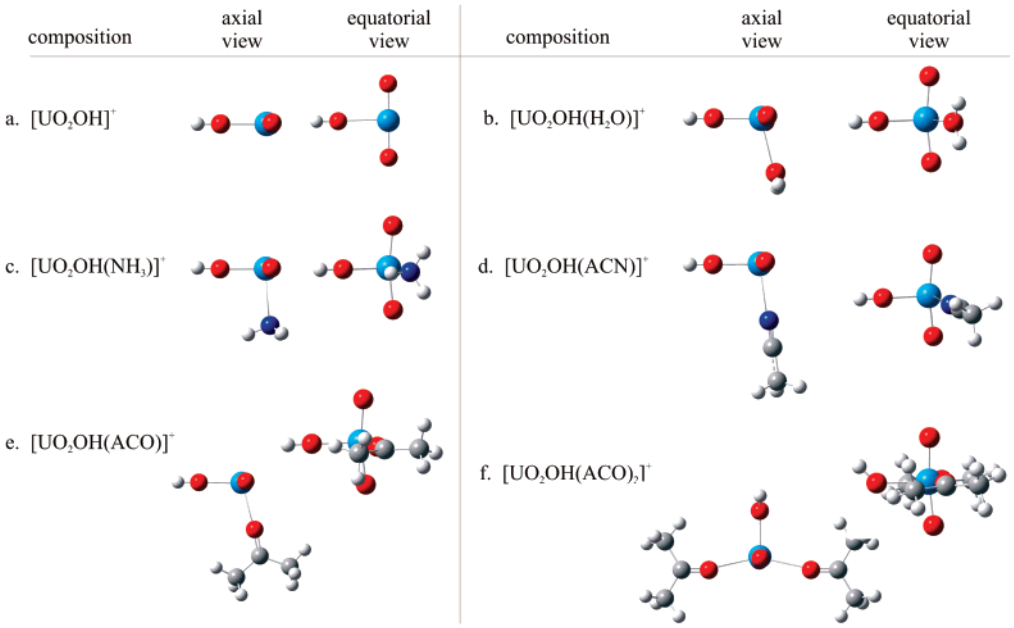

Figure 8. Lowest-energy conformations of calculated for $[UO_2OH]^+$ and its solvated complexes. Calculations were performed using the hybrid B3LYP functional with the Stuttgart RSC/3-21g* basis set approach.

TABLE 5: Bond Lengths and O═U═O Bond Angles for $[UO_2AS]^+$ Complexes at the B3LYP Level of Theory and Using the Stuttgart RSC/3-21g* Basis Set

A (anion)	S (neutral solvent)	U═O length, Å	U−anion length, Å	U−neutral length, Å	O═U═O angle (deg)
$[UO_2]^{2+}$, unligated	n/a	1.700	n/a	n/a	179.6
OAc	n/a	1.744	2.269	n/a	170.3
OAc	H_2O	1.774	2.297	2.462	171.0
OAc	NH_3	1.754	2.302	2.557	171.7
OH	n/a	1.745	2.010	n/a	167.4
OH	H_2O	1.755	2.028	2.442	167.6
OH	NH_3	1.758	2.033	2.544	167.2
OH	ACN	1.757	2.032	2.477	167.0
OH	ACO	1.759	2.005	2.325	169.9
OH	$(ACO)_2$	1.768	2.083	2.393	172.6
OCH_3	n/a	1.751	1.999	n/a	167.2
OCH_3	H_2O	1.762	2.017	2.451	167.6
OCH_3	NH_3	1.763	2.021	2.556	167.2

subsequent addition of a neutral solvent S is very similar for the acetate, the hydroxy, and the methoxide complexes. The uranyl bond elongates by 0.042, 0.044, and 0.048 Å for OAc^-, OH^-, and OCH_3^-, respectively. This is also the order of increasing anion basicity, resulting in donation of more electron density to the uranium atom, and attendant repulsion of the axial oxygen atoms. The amount of donation was quantified by performing charge analysis calculations with PW91/ZORA/TZ2P. The Hirshfeld method shows donation to uranyl of 0.56e (OAc), 0.53e (OH), and 0.65e (OCH_3), and the VDD method gives very similar values of 0.53, 052, and 0.63e, respectively.

The addition of a neutral donor to the uranyl anion complexes induces a further lengthening of the uranyl bonds (Figure 10), by 0.011−0.016 Å, with the largest shifts occurring for the more basic neutrals: in this study, addition of ACO caused the largest O═U═O elongation, consistent with the low uranyl frequency measured in the IRMPD spectrum. The magnitude of the elongation on addition of a neutral is much less than that calculated for the initial attachment of the anion. Hirshfeld analysis showed that the strongest donating neutral species, acetone, donates 0.17 e (for one acetone) or 0.25 e (for two acetones) to a uranyl hydroxide unit in the $[UO_2OH(ACO)_{1,2}]^+$complexes (which have the greatest O═U═O elongation); these values are significantly lower than those calculated for the anions.

The calculations also predict that the uranium-anion distance will be lengthened by addition of a neutral ligand, which is shown by the middle three traces in Figure 10. Increases ranging from 0.017 to 0.024 Å occurred in the U−OH length for the hydroxide complexes, with the magnitude depending on the basicity of the neutral, and the largest elongation being for addition of ACO. When a second ACO is added, the U−OH distance elongates by another 0.036 Å. The $U-OCH_3$ bond distance experiences very nearly identical increases upon addition of H_2O and NH_3 to $[UO_2OCH_3]^+$. The U-anion distance calculated for the acetate complex is substantially longer than that for either the hydroxide or the methoxide, and the B3LYP calculations indicated a bidentate-bound acetate, although calculation using the LDA and the DNP basis set suggested a monodentate structure. Using either approach, the U-acetate length is nearly 0.27 Å longer than for the hydroxide or methoxide. Addition of H_2O or NH_3 to the complex causes elongation of the U-acetate bonds by ∼0.04 and 0.02 Å, respectively. The fact that H_2O produced a longer U-anion elongation than NH_3 is contrary to what would be expected on the basis of calculated coordination energies (NH_3 ∼9 kcal/mol greater than H_2O)[40] but may be consistent with the fact that uranyl behaves as a hard acid,[6,40] interacting more strongly with the oxygen donors.

The U−S bond length in $[UO_2AS]^+$ increased when NH_3 was substituted for H_2O, for all three anions studied. Further U-neutral bond length comparisons involved only the hydroxide and decreased in the order NH_3 > ACN > ACO, minimizing at 2.27 Å. The trend correlates inversely with increasing ligand nucleophilicity. Addition of a second ACO as the third equatorial ligand in $[UO_2OH(ACO)_2]^+$ loosens the overall complex: the U-neutral bond is lengthened by nearly 0.06 Å, and this is accompanied by a lengthening of the U−OH bond by 0.036 Å, and the O═U═O bond by nearly 0.01 Å. As the coordination sphere is completed, distortions of the O═U═O angle from linearity are lessened, and the value approaches 180°.

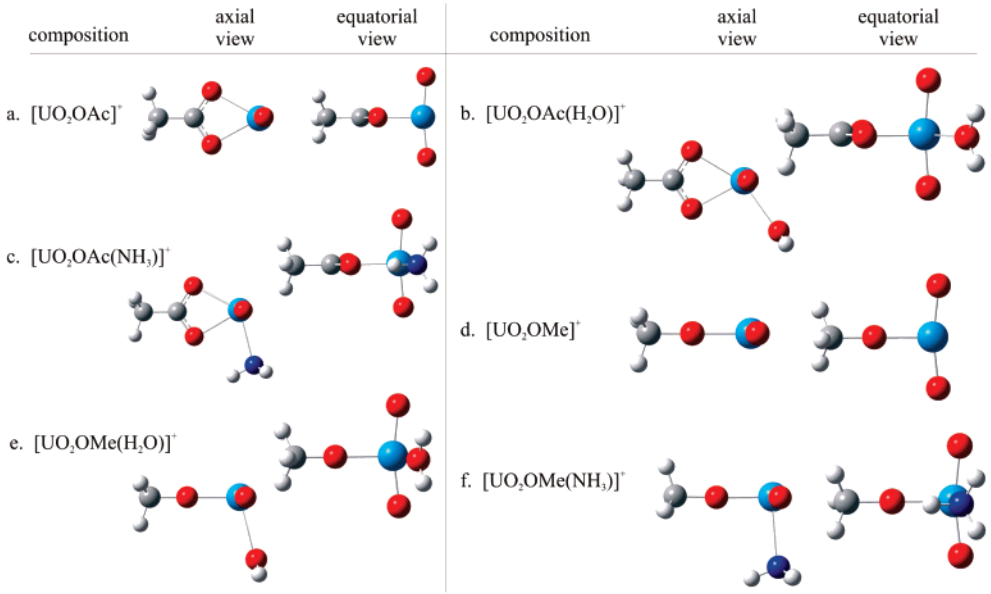

Figure 9. Lowest-energy conformations of $[UO_2OAc]^+$, $[UO_2OMe]^+$, and their solvent complexes with water and ammonia. Calculations were performed using hybrid B3LYP functional with the Stuttgart RSC/3-21g* basis set approach.

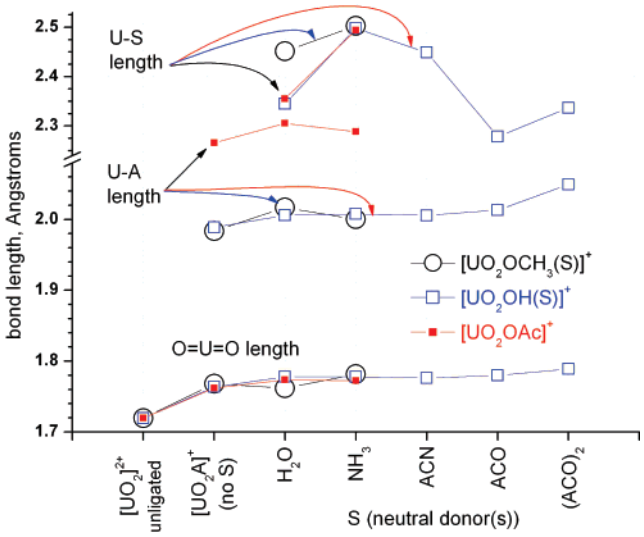

Figure 10. Bond lengths plotted versus neutral for $[UO_2AS]^+$ complexes. Values for unligated $[UO_2]^{2+}$ and $[UO_2A]^+$ complexes are also included. Values were calculated using B3LYP functional and the Stuttgart RSC/3-21g* basis set approach. (Note break in *y* axis at 2.08 Å.)

Conclusions

The structure of uranium complexes has been a persistent topic of research in the chemical community because the participation of 5f, 6d, and 7s orbitals offers a broad array of possible structures and reaction pathways. The desire to understand and then manipulate uranium chemistry has motivated determined investigations of structure and bonding using spectroscopy and computational chemistry. In principle, these approaches should be highly complementary, but in practice, results from each cannot be correlated with each other because spectroscopy measurements on condensed-phase systems almost always measure an ensemble of species, whereas calculations produce data for single discrete species, and do not always include specific and/or long-range interactions with solvent. Consequently, it is difficult to use condensed-phase spectroscopic measurements to evaluate computational accuracy, which is badly needed for molecules containing f elements. Infrared spectra of gas-phase complexes generated using IRMPD provide data for discrete species that are of great value for evaluating ligand binding trends and computational chemistry results.

Much emphasis has been placed on the study of uranyl dication complexes, and our prior IRMPD studies of ACO complexes enabled comparison of antisymmetric O═U═O and C═O frequencies with solution-phase measurements and computational results.[60] However, at mid-pH ranges, uranyl−anion pairs are more prevalent, and hence in the present study, IRMPD of ion pairs involving hydroxide, acetate, and methoxide were examined. The uranyl antisymmetric frequency values were red-shifted equal to or greater than UO_2^{2+} coordinated with four or five neutral donor ligands. Although vibrational anharmonicity no doubt contributes to these low-frequency values, the intrinsic frequencies of the ion pair complexes are lower than expected when compared with solution-phase measurements and with past and present DFT results. The addition of a solvent neutral S to the ion pairs did not result in systematic decreases in the ν_3 values. But when frequencies for the $[UO_2AS]^+$ species were compared for differing neutrals, the ν_3 value decreased with increasing S nucleophilicity, consistent with theory, intuition, and previous IRMPD measurements.[60]

The $[UO_2OCH_3]^+$ molecule underwent wavelength-specific fragmentation reactions, eliminating the OCH_3 radical at a frequency 20 cm^{-1} lower than fragmentations involving rearrangement and or loss of H atom(s). DFT modeling suggested that the OCH_3 radical loss was activated by absorption at the uranyl stretching frequency, and the H atom loss/rearrangement eliminations were activated by absorption at the C−O stretching frequency. Identifying the cause of this phenomenon remains an outstanding task: IRMPD anharmonicity together with absorption nonlinearities (as observed in the spectra of the *para*-aminobenzoic acid cation[58] and $[CeOH(ACO)_{n=3,4}]^{2+}$ cation[95]) may contribute to the phenomenon; however, the very large differences in the different photofragmentation channels suggests that there may be another factor at work, such as promotion to an excited-state electronic configuration, which would be energetically feasible.

Acknowledgment. Work by G. S. G. and A. K. G. was supported by the U.S. Department of Energy, Assistant Secretary for Environmental Management, and the INL Laboratory Directed Research & Development Program under DOE Idaho Operations Office Contract DE-AC07-05ID14517. M.J.V.S was supported in part through a grant from the U.S. National Science Foundation (CAREER-0239800). Gaussian 03 calculations were performed at the Wichita State University High-performance Computing Center (HIPECC), a facility supported by the U.S. National Science Foundation under Grant No. EIA-0216178 and Grant No. EPS-0236913, with matching support from the State of Kansas and HIPECC. W.A.d.J.'s research was performed, in part, using the Molecular Science Computing Facility in the William R. Wiley Environmental Molecular Sciences Laboratory, a national scientific user facility sponsored by the U.S. Department of Energy's Office of Biological and Environmental Research located at the Pacific Northwest National Laboratory, which is operated for the Department of Energy by Battelle. The FOM authors, and authors from V.U.A., were supported by the Nederlandse Organisatie voor Wetenschappelijk Onderzoek (Dutch National Science Foundation). The skillful assistance by the FELIX staff, in particular Dr. B. Redlich, is gratefully acknowledged. Construction and shipping of the FTMS instrument was made possible through funding from the National High Field FT-ICR Facility (grant CHE-9909502) at the National High Magnetic Field Laboratory, Tallahassee, FL, as was travel support for one of the INL authors; John Eyler's assistance was particularly invaluable.

Supporting Information Available: Complete listings of structural data (frequencies, bond lengths and angles) calculated using B3LYP with the Stuttgart RSC/D95V, and Stuttgart RSC/3-21g* basis sets are provided in tables S1−S12. Geometries of molecular structures in xyz format. This material is available free of charge via the Internet at http://pubs.acs.org.

References and Notes

(1) Choppin, G. R.; Rizkalla, E. N. Solution Chemistry of Actinides and Lanthanides. In *Handbook on the Physics and Chemistry of Rare Earths*; Gschneider, J., K. A., Eyring, L., Choppin, G. R., Lander, G. H., Eds.; Vol. 18, Lanthanides/Actinides: Chemistry; North-Holland: Amsterdam, 1994; pp 559.

(2) Denning, R. G. *Struct. Bonding* **1992**, *79*, 215.

(3) Pepper, M.; Bursten, B. E. *Chem. Rev.* **1991**, *91*, 719.

(4) Matsika, S.; Zhang, Z.; Brozell, S. R.; Blaudeau, J.-P.; Wang, Q.; Pitzer, R. M. *J. Phys. Chem. A* **2001**, *105*, 3825.

(5) Silva, R. J.; Nitsche, H. *Radiochim. Acta* **1995**, *70/71*, 377

(6) Morse, J. W.; Choppin, G. R. *Rev. Aquatic Sci.* **1991**, *4*, 1.

(7) Toth, L. M.; Begun, G. M. *J. Phys. Chem.* **1981**, *85*, 547.

(8) Burgess, J. *Metal Ions in Solution*; Ellis Horwood Limited: Chichester, U.K., 1978.

(9) Choppin, G. *Radiochim. Acta* **2004**, *92*, 519.

(10) Brookins, D. G. *Geochemical Aspects of Radioactive Waste Disposal*; Springer-Verlag: New York, 1984.
(11) Rizkalla, E. N.; Choppin, G. R. Lanthanides and Actinides Hydration and Hydrolysis. In *Handbook on the Physics and Chemistry of Rare Earths. Volume 18: Lanthanides/Actinides: Chemistry*; Gschneidner, J. K. A., Eyring, L., Choppin, G. R., Lander, G. H., Eds.; North-Holland: New York, 1994; Vol. 18, pp 529.
(12) Nguyen-Trung, C.; Palmer, D. A.; Begun, G. M.; Peiffert, C.; Mesmer, R. E. *J. Solution Chem.* **2000**, *29*, 101.
(13) Brooker, M. H.; Huang, C.-H.; Sylwestrowicz, J. *J. Inorg. Nucl. Chem.* **1980**, *42*, 1431.
(14) Glebov, V. A. *Koord. Khim.* **1982**, *8*, 970.
(15) Nguyen-Trung, C.; Begun, G. M.; Palmer, D. A. *Inorg. Chem.* **1992**, *31*, 5280.
(16) Jones, L. H. *Spectrochim. Acta* **1958**, *10*, 395.
(17) Quiles, F.; Burneau, A. *Vibr. Spectrosc.* **1998**, *18*, 61.
(18) Gal, M.; Goggin, P. L.; Mink, J. *J. Mol. Struct.* **1984**, *114*, 459.
(19) McGlynn, S. P.; Smith, J. K.; Neely, W. C. *J. Chem. Phys.* **1961**, *35*, 105.
(20) Jones, L. H.; Penneman, R. A. *J. Chem. Phys.* **1953**, *21*, 542.
(21) Best, S. P.; Clark, R. J. H.; Cooney, R. P. *Inorg. Chim. Acta* **1988**, *145*, 141.
(22) Clark, D. L.; Conradson, S. D.; Donohoe, R. J.; Keogh, D. W.; Morris, D. E.; Palmer, P. D.; Rogers, R. D.; Tait, C. D. *Inorg. Chem.* **1999**, *38*, 1456.
(23) Kakihana, M.; Nagumo, T.; Okamoto, M.; Kakihana, H. *J. Phys. Chem.* **1987**, *91*, 6128.
(24) Mizuoka, K.; Ikeda, Y. *Radiochim. Acta* **2004**, *92*, 631.
(25) Burns, C. J.; Smith, C. C.; Sattelberger, A. P.; Gray, H. B. *Inorg. Chem.* **1992**, *31*, 3724.
(26) Morris, D. E.; Chisholm-Brause, C. J.; Barr, M. E.; Conradson, S. D.; Gary Eller, P. *Geochim. Cosmochim. Acta* **1994**, *58*, 3613.
(27) Duff, M. C.; Coughlin, J. U.; Hunter, D. B. *Geochim. Cosmochim. Acta* **2002**, *66*, 3533.
(28) Tellez Soto, C. A.; Arissawa, M.; Gomez, L., J.; Mondragon, M. A. *Polyhedron* **2000**, *19*, 2353.
(29) Madic, C.; Hobart, D. E.; Begun, G. M. *Inorg. Chem.* **1983**, *22*, 1494.
(30) Glebov, V. A. *Koord. Khim.* **1981**, *7*, 388.
(31) Mizuoka, K.; Ikeda, Y. *Inorg. Chem.* **2003**, *42*, 3396.
(32) Basile, L. J.; Sullivan, J. C.; Ferraro, J. R.; LaBonville, P. *Appl. Spectrosc.* **1974**, *28*, 142.
(33) Schreckenbach, G.; Hay, P. J.; Martin, R. L. *J. Comput. Chem.* **1999**, *20*, 70.
(34) Vetere, V.; Maldivi, P.; Adamo, C. *J. Comput. Chem.* **2003**, *24*, 850.
(35) Van Wullen, C. *J. Comput. Chem.* **1999**, *20*, 51.
(36) Kaltsoyannis, N. *Chem. Soc. Rev.* **2003**, *32*, 9.
(37) de Jong, W. A.; Harrison, R. J.; Nichols, J. A.; Dixon, D. A. *Theor. Chem. Acc.* **2001**, *107*, 22.
(38) Clavaguera-Sarrio, C.; Ismail, N.; Marsden, C. J.; Begue, D.; Pouchan, C. *Chem. Phys.* **2004**, *302*, 1.
(39) Hay, P. J.; Martin, R. L.; Schreckenbach, G. *J. Phys. Chem. A* **2000**, *104*, 6259.
(40) Clavaguera-Sarrio, C.; Hoyau, S.; Ismail, N.; Marsden, C. J. *J. Phys. Chem. A* **2003**, *107*, 4515.
(41) Farkas, I.; Banyai, I.; Szabo, Z.; Wahlgren, U.; Grenthe, I. *Inorg. Chem.* **2000**, *39*, 799.
(42) Gutowski, K. E.; Dixon, D. A. *J. Phys. Chem. A* **2006**, *110*, 8840.
(43) Gutowski, K. E.; Cocalia, V. A.; Griffin, S. T.; Bridges, N. J.; Dixon, D. A.; Rogers, R. D. *J. Am. Chem. Soc.* **2007**, *129*, 526.
(44) Duncan, M. A. *Int. Rev. Phys. Chem.* **2003**, *22*, 407.
(45) Lemaire, J.; Boissel, P.; Heninger, M.; Mauclaire, G.; Bellec, G.; Mestdagh, H.; Simon, A.; Le Caer, S.; Ortega, J. M.; Glotin, F.; Maitre, P. *Phys. Rev. Lett.* **2002**, *89*.
(46) Moore, D. T.; Oomens, J.; Eyler, J. R.; Meijer, G.; von Helden, G.; Ridge, D. P. *J. Am. Chem. Soc.* **2004**, *126*, 14726.
(47) Oepts, D.; van der Meer, A. F. G.; van Amersfoort, P. W. *Infrared Phys. Technol.* **1995**, *36*, 297.
(48) Fenn, J. B.; Mann, M.; Meng, C. K.; Wong, S. F.; Whitehouse, C. M. *Science* **1989**, *246*, 64.
(49) Schroder, D.; Roithova, J.; Schwarz, H. *Int. J. Mass Spectrom.* **2006**, *254*, 197.
(50) Stewart, I. I. *Spectrochim. Acta, Part B* **1999**, *54*, 1649.
(51) Gatlin, C. L.; Turecek, F. Electrospray Ionization of Inorganic and Organometallic Complexes. In *Electrospray Ionization Mass Spectrometry*; John Wiley & Sons: New York, 1997; pp 527.
(52) Chien, W.; Anbalagan, V.; Zandler, M.; Hanna, D.; Van, Stipdonk, M.; Gresham, G.; Groenewold, G. *J. Am. Soc. Mass Spectrom.* **2004**, *15*, 777.
(53) Van Stipdonk, M.; Anbalagan, V.; Chien, W.; Gresham, G.; Groenewold, G.; Hanna, D. *J. Am. Soc. Mass Spectrom.* **2003**, *14*, 1205.
(54) Van Stipdonk, M. J.; Chien, W.; Angalaban, V.; Bulleigh, K.; Hanna, D.; Groenewold, G. S. *J. Phys. Chem. A* **2004**, *108*, 10448.
(55) Van Stipdonk, M. J.; Chien, W.; Bulleigh, K.; Wu, Q.; Groenewold, G. S. *J. Phys. Chem. A* **2006**, *110*, 959.
(56) Oomens, J.; Sartakov, B. G.; Meijer, G.; von Helden, G. *Int. J. Mass Spectrom.* **2006**, *254*, 1.
(57) Moore, D. T.; Oomens, J.; van der Meer, L.; von Helden, G.; Meijer, G.; Valle, J.; Marshall, A. G.; Eyler, J. R. *Chem. Phys. Chem.* **2004**, *5*, 740.
(58) Oomens, J.; Moore, D. T.; Meijer, G.; von Helden, G. *Phys. Chem. Chem. Phys.* **2004**, *6*, 710.
(59) Oomens, J.; Moore, D. T.; von Helden, G.; Meijer, G.; Dunbar, R. C. *J. Am. Chem. Soc.* **2004**, *126*, 724.
(60) Groenewold, G. S.; Gianotto, A. K.; Cossel, K. C.; Van, Stipdonk, M. J.; Moore, D. T.; Polfer, N.; Oomens, J.; de Jong, W. A.; Visscher, L. *J. Am. Chem. Soc.* **2006**, *107*, 4802.
(61) Sachs, S.; Brendler, V.; Geipel, G. *Radiochim. Acta* **2007**, *95*, 103.
(62) Valle, J. J.; Eyler, J. R.; Oomens, J.; Moore, D. T.; van der Meer, A. F. G.; von Helden, G.; Meijer, G.; Hendrickson, C. L.; Marshall, A. G.; Blakney, G. T. *Rev. Sci. Instrum.* **2005**, *76*, 023103.
(63) Marshall, A. G.; Wang, T.-C. L.; Ricca, T. L. *J. Am. Chem. Soc.* **1985**, *107*, 7893.
(64) Bagratashivili, V. N.; Letokov, V. S.; Makarov, A. A.; Ryabov, E. A. *Mutiple Photon Infrared Laser Photophysics and Photochemistry*; Harwood: Chur, Switzerland, 1985.
(65) Oomens, J.; Tielens, A. G. G. M.; Sartakov, B. G.; Von, Helden, G.; Meijer, G. *Astrophys. J.* **2003**, *591*, 968.
(66) Marshall, A. G. *Acc. Chem. Res.* **1985**, *18*, 316.
(67) Marshall, A. G.; Hendrickson, C. L.; Jackson, G. S. *Mass Spectrom. Rev.* **1998**, *17*, 1.
(68) Delley, B. *J. Chem. Phys.* **1990**, *92*, 508.
(69) Delley, B. *J. Chem. Phys.* **2000**, *113*, 7756.
(70) Aprà, E.; et.al. NWChem, A Computational Chemistry Package for Parallel Computers, Version 4.7 ed.; Pacific Northwest National Laboratory: Richland, WA, 99352−0999, U.S.A., 2005.
(71) Kendall, R. A.; Apra, E.; Bernholdt, D. E.; Bylaska, E. J.; Dupuis, M.; Fann, G. I.; Harrison, R. J.; Ju, J.; Nichols, J. A.; Nieplocha, J.; Straatsma, T. P.; Windus, T. L.; Wong, A. T. *Comput. Phys. Commun.* **2000**, *128*, 260.
(72) Frisch, M. J.; Trucks, G. W.; Schlegel, H. B.; Scuseria, G. E.; Robb, M. A.; Cheeseman, J. R.; Zakrzewski, V. G.; Montgomery, J. A., Jr.; Stratmann, R. E.; Burant, J. C.; Dapprich, S.; Millam, J. M.; Daniels, A. D.; Kudin, K. N.; Strain, M. C.; Farkas, O.; Tomasi, J.; Barone, V.; Cossi, M.; Cammi, R.; Mennucci, B.; Pomelli, C.; Adamo, C.; Clifford, S.; Ochterski, J.; Petersson, G. A.; Ayala, P. Y.; Cui, Q.; Morokuma, K.; Malick, D. K.; Rabuck, A. D.; Raghavachari, K.; Foresman, J. B.; Cioslowski, J.; Ortiz, J. V.; Stefanov, B. B.; Liu, G.; Liashenko, A.; Piskorz, P.; Komaromi, I.; Gomperts, R.; Martin, R. L.; Fox, D. J.; Keith, T.; Al-Laham, M. A.; Peng, C. Y.; Nanayakkara, A.; Gonzalez, C.; Challacombe, M.; Gill, P. M. W.; Johnson, B.; Chen, W.; Wong, M. W.; Andres, J. L.; Gonzalez, C.; Head-Gordon, M.; Replogle, E. S.; Pople, J. A. *Gaussion 98*, revision A.4; Gaussian, Inc.: Pittsburgh, PA, 1998.
(73) te Velde, G.; Bickelhaupt, F. M.; Baerends, E. J.; Guerra, C. F.; Van, Gisbergen, S. J. A.; Snijders, J. G.; Ziegler, T. *J. Comput. Chem.* **2001**, *22*, 931.
(74) Slater, J. C. *Phys. Rev. Lett.* **1951**, *81*, 385.
(75) Vosko, S. J.; Wilk, W.; Nusair, M. *Can. J. Phys.* **1980**, *58*, 1200.
(76) Becke, A. D. *J. Chem. Phys.* **1993**, *98*, 5648.
(77) Lee, C. T.; Yang, W. T.; Parr, R. G. *Phys. Rev. B* **1988**, *37*, 785.
(78) Perdew, J. P.; Chevary, J. A.; Vosko, S. H.; Jackson, K. A.; Pederson, M. R.; Singh, D. J.; Fiolhais, C. **1992**, *46*, 6671.
(79) Delley, B. *Int. J. Quantum Chem.* **1998**, *69*, 423.
(80) Ortiz, J. V.; Hay, P. J.; Martin, R. L. *J. Am. Chem. Soc.* **1992**, *114*, 2736.
(81) Bergner, A.; Dolg, M.; Kuchle, W.; Stoll, H.; Preuss, H. *Mol. Phys.* **1993**, *80*, 1431.
(82) Dolg, M. *Modern Methods and Algorithms of Quantum Chemistry*; John von Neumann Institute for Computing: Julich, Germany, 2000; Vol. 1.
(83) Dunning, T. H., Jr.; Hay, P. H. *Modern Theoretical Chemistry*; Plenum: New York, 1976; Vol. 3.
(84) Kuchle, W.; Dolg, M.; Stoll, H.; Preuss, H. *Mol. Phys.* **1991**, *74*, 1245.
(85) Dunning, T. H. *J. Chem. Phys.* **1989**, *90*, 1007.
(86) van Lenthe, E.; Baerends, E. J.; Snijders, J. G. *J. Chem. Phys.* **1993**, *99*, 4597.
(87) Chaban, G. M.; Jung, J. O.; Gerber, R. B. *J. Chem. Phys.* **1999**, *111*, 1823.
(88) Matsunaga, N.; Chaban, G. M.; Gerber, R. B. *J. Chem. Phys.* **2002**, *117*, 3541.
(89) Yagi, K.; Hirao, K.; Taketsugu, T.; Schmidt, M. W.; Gordon, M. S. *J. Chem. Phys.* **2004**, *121*, 1383.
(90) Hirshfeld, F. L. *Theor. Chim. Acta* **1977**, *44*, 129.

(91) Fonseca Guerra, C.; Handgraaf, J.-W.; Baerends, E. J.; Bickelhaupt, F. M. *J. Comput. Chem.* **2004**, *25*, 189.

(92) Soderholm, L.; Skanthakumar, S.; Neuefeind, J. *Anal. Bioanal. Chem.* **2005**, *383*, 48.

(93) Neuefeind, J.; Soderholm, L.; Skanthakumar, S. *J. Phys. Chem. A* **2004**, *108*, 2733.

(94) Quiles, F.; Burneau, A. *Vibr. Spectrosc.* **2000**, *23*, 231.

(95) Groenewold, G. S.; Gianotto, A. K.; Cossel, K. C.; Van Stipdonk, M. J.; Oomens, J.; Polfer, N.; Moore, D. T.; de Jong, W. A.; McIlwain, M. E. *Phys. Chem. Chem. Phys.* **2006**, *9*, 596.

(96) Kasha, M. *J. Chem. Phys.* **1949**, *17*, 349.

(97) Lias, S. G. NIST Chemistry WebBook; United States Department of Commerce, National Institute of Standards and Technology, 2003; Vol. 2004.

(98) de Jong, W. A.; Apra, E.; Windus, T. L.; Nichols, J. A.; Harrison, R. J.; Gutowski, K. E.; Dixon, D. A. *J. Phys. Chem. A* **2005**, *109*, 11568.

(99) Rodgers, M. T.; Armentrout, P. B. *Mass Spectrom. Rev.* **2000**, *19*, 215.